Raman self-frequency-shift of soliton crystal in a high index doped silica micro-ring resonator [Invited]

Lu, Zhizhou; Wang, Weiqiang; Zhang, Wenfu; Liu, Mulong; Wang, Leiran; Chu, Sai T.; Little, Brent E.; Zhao, Jianguo; Xie, Peng; Wang, Xinyu; Zhao, Wei

Published in:
Optical Materials Express

Published: 01/09/2018

Document Version:
Final Published version, also known as Publisher's PDF, Publisher's Final version or Version of Record

License:
Unspecified

Publication record in CityU Scholars:
Go to record

Published version (DOI):
10.1364/OME.8.002662

Publication details:
Lu, Z., Wang, W., Zhang, W., Liu, M., Wang, L., Chu, S. T., Little, B. E., Zhao, J., Xie, P., Wang, X., & Zhao, W. (2018). Raman self-frequency-shift of soliton crystal in a high index doped silica micro-ring resonator [Invited]. *Optical Materials Express*, *8*(9), 2662-2669. https://doi.org/10.1364/OME.8.002662

Research Article | Vol. 8, No. 9 | 1 Sep 2018 | OPTICAL MATERIALS EXPRESS 2662
Optical Materials EXPRESS

Raman self-frequency-shift of soliton crystal in a high index doped silica micro-ring resonator [Invited]

ZHIZHOU LU,[1,2] WEIQIANG WANG,[1,2,5] WENFU ZHANG,[1,2,6] MULONG LIU,[1,2] LEIRAN WANG,[1,2] SAI T. CHU,[3] BRENT E. LITTLE,[1] JIANGUO ZHAO,[4] PENG XIE,[1,2] XINYU WANG,[1,2] AND WEI ZHAO[1,2]

[1]*State Key Laboratory of Transient Optics and Photonics, Xi'an Institute of Optics and Precision Mechanics (XIOPM), Chinese Academy of Sciences (CAS), Xi'an 710119, China*
[2]*University of Chinese Academy of Sciences, Beijing 100049, China*
[3]*Department of Physics and Materials Science, City University of Hong Kong, Hong Kong, China*
[4]*Chair of Micromechanics, Microfluidics/Microactuators, Saarland University, Saarbrücken 66123, Germany*
[5]*wwq@opt.ac.cn*
[6]*wfuzhang@opt.ac.cn*

Abstract: High index doped silica glass exhibiting low loss property and CMOS compatibility is a promising material in nonlinear optics. In this work, mode-locked soliton crystals (SCs) are demonstrated in a high-Q (>10^6) micro-ring resonator (MRR) made in this platform. The asymmetric spectra of SCs are numerically investigated and interpreted as the combined impact of Raman self-frequency shift (RSFS) and the wavelength-dependent loss. By precisely comparing the experimental and simulated spectra based on the perturbed Lugiato-Lefever equation (LLE), the Raman shock time is inferred to be at the range of 2.5 fs to 2.7 fs for this material.

OCIS codes: (190.4380) Nonlinear optics, four-wave mixing; (190.3270) Kerr effect; (190.4360) Nonlinear optics, devices; (190.4400) Nonlinear optics, materials; (140.3945) Microcavities.

References and links

1. K. J. Vahala, "Optical microcavities," Nature **424**(6950), 839–846 (2003).
2. D. K. Armani, T. J. Kippenberg, S. M. Spillane, and K. J. Vahala, "Ultra-high-Q toroid microcavity on a chip," Nature **421**(6926), 925–928 (2003).
3. R. Henriet, G. Lin, A. Coillet, M. Jacquot, L. Furfaro, L. Larger, and Y. K. Chembo, "Kerr optical frequency comb generation in strontium fluoride whispering-gallery mode resonators with billion quality factor," Opt. Lett. **40**(7), 1567–1570 (2015).
4. T. J. Kippenberg, S. M. Spillane, and K. J. Vahala, "Kerr-nonlinearity optical parametric oscillation in an ultrahigh-Q toroid microcavity," Phys. Rev. Lett. **93**(8), 083904 (2004).
5. G. P. Agrawal, Nonlinear Fiber Optics (Academic Press, 2007).
6. W. Wang, S. T. Chu, B. E. Little, A. Pasquazi, Y. Wang, L. Wang, W. Zhang, L. Wang, X. Hu, G. Wang, H. Hu, Y. Su, F. Li, Y. Liu, and W. Zhao, "Dual-pump Kerr Micro-cavity Optical Frequency Comb with varying FSR spacing," Sci. Rep. **6**(1), 28501 (2016).
7. Q.-T. Cao, H. Wang, C.-H. Dong, H. Jing, R.-S. Liu, X. Chen, L. Ge, Q. Gong, and Y.-F. Xiao, "Experimental demonstration of spontaneous chirality in a nonlinear microresonator," Phys. Rev. Lett. **118**(3), 033901 (2017).
8. L. Del Bino, J. M. Silver, S. L. Stebbings, and P. Del'Haye, "Symmetry breaking of counter-propagating light in a nonlinear resonator," Sci. Rep. **7**(1), 43142 (2017).
9. Y. Chen, Z.-H. Zhou, C.-L. Zou, Z. Shen, G.-C. Guo, and C.-H. Dong, "Tunable Raman laser in a hollow bottle-like microresonator," Opt. Express **25**(14), 16879–16887 (2017).
10. X. Guo, C.-L. Zou, H. Jung, and H. X. Tang, "On-Chip Strong Coupling and Efficient Frequency Conversion between Telecom and Visible Optical Modes," Phys. Rev. Lett. **117**(12), 123902 (2016).
11. T. Herr, V. Brasch, J. D. Jost, C. Y. Wang, N. M. Kondratiev, M. L. Gorodetsky, and T. J. Kippenberg, "Temporal solitons in optical microresonators," Nat. Photonics **8**(2), 145–152 (2014).
12. V. Brasch, M. Geiselmann, T. Herr, G. Lihachev, M. H. Pfeiffer, M. L. Gorodetsky, and T. J. Kippenberg, "Photonic chip-based optical frequency comb using soliton Cherenkov radiation," Science **351**(6271), 357–360 (2016).

#335744 https://doi.org/10.1364/OME.8.002662
Journal © 2018 Received 20 Jun 2018; accepted 30 Jul 2018; published 15 Aug 2018

13. X. Yi, Q.-F. Yang, K. Y. Yang, M.-G. Suh, and K. Vahala, "Soliton frequency comb at microwave rates in a high-Q silica microresonator," Optica **2**(12), 1078 (2015).
14. P. H. Wang, J. A. Jaramillo-Villegas, Y. Xuan, X. Xue, C. Bao, D. E. Leaird, M. Qi, and A. M. Weiner, "Intracavity characterization of micro-comb generation in the single-soliton regime," Opt. Express **24**(10), 10890–10897 (2016).
15. C. Joshi, J. K. Jang, K. Luke, X. Ji, S. A. Miller, A. Klenner, Y. Okawachi, M. Lipson, and A. L. Gaeta, "Thermally controlled comb generation and soliton modelocking in microresonators," Opt. Lett. **41**(11), 2565–2568 (2016).
16. Q. Li, T. C. Briles, D. A. Westly, T. E. Drake, J. R. Stone, B. R. Ilic, S. A. Diddams, S. B. Papp, and K. Srinivasan, "Stably accessing octave-spanning microresonator frequency combs in the soliton regime," Optica **4**(2), 193–203 (2017).
17. A. Pasquazi, M. Peccianti, L. Razzari, D. J. Moss, S. Coen, M. Erkintalo, Y. K. Chembo, T. Hansson, S. Wabnitz, P. Del'Haye, X. Xue, A. M. Weiner, and R. Morandotti, "Micro-Combs: A Novel Generation of Optical Sources," Phys. Rep. **729**(1), 1–81 (2018).
18. X. Xu, J. Wu, T. G. Nguyen, M. Shoeiby, S. T. Chu, B. E. Little, R. Morandotti, A. Mitchell, and D. J. Moss, "Advanced RF and microwave functions based on an integrated optical frequency comb source," Opt. Express **26**(3), 2569–2583 (2018).
19. M. G. Suh and K. J. Vahala, "Soliton microcomb range measurement," Science **359**(6378), 884–887 (2018).
20. P. Trocha, M. Karpov, D. Ganin, M. H. P. Pfeiffer, A. Kordts, S. Wolf, J. Krockenberger, P. Marin-Palomo, C. Weimann, S. Randel, W. Freude, T. J. Kippenberg, and C. Koos, "Ultrafast optical ranging using microresonator soliton frequency combs," Science **359**(6378), 887–891 (2018).
21. M. G. Suh, Q. F. Yang, K. Y. Yang, X. Yi, and K. J. Vahala, "Microresonator soliton dual-comb spectroscopy," Science **354**(6312), 600–603 (2016).
22. M. Yu, Y. Okawachi, A. G. Griffith, N. Picqué, M. Lipson, and A. L. Gaeta, "Silicon-chip-based mid-infrared dual-comb spectroscopy," Nat. Commun. **9**(1), 1869 (2018).
23. P. Marin-Palomo, J. N. Kemal, M. Karpov, A. Kordts, J. Pfeifle, M. H. P. Pfeiffer, P. Trocha, S. Wolf, V. Brasch, M. H. Anderson, R. Rosenberger, K. Vijayan, W. Freude, T. J. Kippenberg, and C. Koos, "Microresonator-based solitons for massively parallel coherent optical communications," Nature **546**(7657), 274–279 (2017).
24. Y. Geng, X. Huang, W. Cui, Y. Ling, B. Xu, J. Zhang, X. Yi, B. Wu, S.-W. Huang, K. Qiu, C. W. Wong, and H. Zhou, "Terabit optical OFDM superchannel transmission via coherent carriers of a hybrid chip-scale soliton frequency comb," Opt. Lett. **43**(10), 2406–2409 (2018).
25. X. Yi, Q. F. Yang, K. Y. Yang, and K. Vahala, "Theory and measurement of the soliton self-frequency shift and efficiency in optical microcavities," Opt. Lett. **41**(15), 3419–3422 (2016).
26. M. Karpov, H. Guo, A. Kordts, V. Brasch, M. H. Pfeiffer, M. Zervas, M. Geiselmann, and T. J. Kippenberg, "Raman self-frequency shift of dissipative kerr solitons in an optical microresonator," Phys. Rev. Lett. **116**(10), 103902 (2016).
27. W. Wang, Z. Lu, W. Zhang, S. T. Chu, B. E. Little, L. Wang, X. Xie, M. Liu, Q. Yang, L. Wang, J. Zhao, G. Wang, Q. Sun, Y. Liu, Y. Wang, and W. Zhao, "Robust soliton crystals in a thermally controlled microresonator," Opt. Lett. **43**(9), 2002–2005 (2018).
28. M. Ferrera, L. Razzari, D. Duchesne, R. Morandotti, Z. Yang, M. Liscidini, J. E. Sipe, S. Chu, B. E. Little, and D. J. Moss, "Low-power continuous-wave nonlinear optics in doped silica glass integrated waveguide structures," Nat. Photonics **2**(12), 737–740 (2008).
29. L. Razzari, D. Duchesne, M. Ferrera, R. Morandotti, S. Chu, B. E. Little, and D. J. Moss, "CMOS-compatible integrated optical hyper-parametric oscillator," Nat. Photonics **4**(1), 41–45 (2010).
30. W. Wang, W. Zhang, S. T. Chu, B. E. Little, Q. Yang, L. Wang, X. Hu, L. Wang, G. Wang, Y. Wang, and W. Zhao, "Repetition rate multiplication pulsed laser source based on a microring resonator," ACS Photonics **4**(6), 1677–1683 (2017).
31. D. J. Moss, R. Morandotti, A. L. Gaeta, and M. Lipson, "New CMOS-compatible platforms based on silicon nitride and Hydex for nonlinear optics," Nat. Photonics **7**(8), 597–607 (2013).
32. T. Herr, V. Brasch, J. D. Jost, I. Mirgorodskiy, G. Lihachev, M. L. Gorodetsky, and T. J. Kippenberg, "Mode spectrum and temporal soliton formation in optical microresonators," Phys. Rev. Lett. **113**(12), 123901 (2014).
33. X. Liu, C. Sun, B. Xiong, L. Wang, J. Wang, Y. Han, Z. Hao, H. Li, Y. Luo, J. Yan, T. Wei, Y. Zhang, and J. Wang, "Integrated high-Q crystalline AlN microresonators for broadband Kerr and Raman frequency combs," ACS Photonics **5**(5), 1943–1950 (2018).
34. Y. Okawachi, M. Yu, V. Venkataraman, P. M. Latawiec, A. G. Griffith, M. Lipson, M. Lončar, and A. L. Gaeta, "Competition between Raman and Kerr effects in microresonator comb generation," Opt. Lett. **42**(14), 2786–2789 (2017).
35. C. Bao, Y. Xuan, C. Wang, J. A. Jaramillo-Villegas, D. E. Leaird, M. Qi, and A. M. Weiner, "Soliton repetition rate in a silicon-nitride microresonator," Opt. Lett. **42**(4), 759–762 (2017).
36. C. Bao, Y. Xuan, D. E. Leaird, S. Wabnitz, M. Qi, and A. M. Weiner, "Spatial mode-interaction induced single soliton generation in microresonators," Optica **4**(9), 1011–1015 (2017).
37. M. Liu, L. Wang, Q. Sun, S. Li, Z. Ge, Z. Lu, W. Wang, G. Wang, W. Zhang, X. Hu, and W. Zhao, "Influences of multiphoton absorption and free-carrier effects on frequency-comb generation in normal dispersion silicon microresonators," Photon. Res. **6**(4), 238–243 (2018).

Optical Materials EXPRESS

38. D. C. Cole, E. S. Lamb, P. Del'Haye, S. A. Diddams, and S. B. Papp, "Soliton crystals in Kerr resonators," Nat. Photonics **11**(10), 671–676 (2017).
39. P. Del'Haye, A. Coillet, W. Loh, K. Beha, S. B. Papp, and S. A. Diddams, "Phase steps and resonator detuning measurements in microresonator frequency combs," Nat. Commun. **6**(1), 5668 (2015).

1. Introduction

Benefiting from the breakthrough in theory and fabrication processing over the last two decades [1,2], optical micro-cavities with Q-factor as high as 10^{11} have been demonstrated [3]. The photon-storage time in such cavities corresponds to hundreds of microseconds, which induces ultra-high optical intensity [4] due to constructive interference inside the cavities and stimulates intriguing nonlinear effects in such system. For the centrosymmetric materials such as Si, Si_3N_4, and SiO_2, the 3rd order nonlinear effect including self-phase modulation (SPM), cross-phase modulation (XPM) and four wave mixing (FWM) [5], are introduced due to the cavity-power-driven field-enhancement effect [6]. These nonlinear effects have been exploited in chirality [7,8], Raman laser [9] and frequency conversion [10]. Recently, researchers' interests have been attracted by another iconic nonlinear phenomena in high-Q micro-cavity, that is, the on-chip soliton micro-comb [11–17], which has been successfully utilized in microwave generation [18], ranging measurement [19,20], dual-comb spectroscopy [21,22], and coherent communication [23,24] with unprecedented precision. Theoretically, dissipative cavity solitons (DCSs) rely on the double balance between anomalous cavity dispersion and Kerr nonlinearity on the one hand, the cavity loss and parametric gain on the other. Meanwhile, the high peak power of such solitons will stimulate high order nonlinear effect, such as Raman effect, which has been demonstrated in former DCS generation experiment [25,26], where DCSs experience the so-called Raman self-frequency shift (RSFS), resulting in asymmetric power-spectra distribution about the pump. Phenomenally, the maximum of spectra is red-shifted away from the pump by a certain amount, which is mainly dependent on the pulse-width, group velocity dispersion (GVD) and material-associated Raman shock time [25].

In this paper, the RSFS effect on soliton crystals (SCs) is numerically and experimentally investigated. The SCs are generated in a high-Q micro-ring resonator (MRR) fabricated on a high-index doped silica glass platform, using thermal-controlled method [27], the spectra exhibiting obvious asymmetric characteristic are obtained. Such asymmetry is caused by the combined contribution from wavelength-dependent loss and RSFS. In order to precisely determine the Raman shock time for this material, the loss term is measured and taken into account in our theoretical model based on the perturbed Lugiato-Lefever equation (LLE). By comparing couples of experimental and simulated optical spectra, Raman shock time between 2.5 fs to 2.7 fs is inferred for this material. This result contributes to the understanding of Kerr frequency combs in the solitons regimes and is relevant to improve the accuracy of numerical simulations.

2. Devices

Figure 1(a) shows the schematic of the add-drop type MRR made of high index doped silica glass (n=1.6) using SiO_2 as cladding. The MRR is fabricated by CMOS-compatible process, the core films are deposited using plasma enhanced chemical vapor deposition (PECVD), and then the device patterns are printed in photoresist using an in-line stepper and reactive ion etching to produce exceptional low sidewall roughness on the core layer [28–31]. The radius of the MRR is 592.1μm , corresponding to the free spectral range (FSR) of ~49 GHz, and the gap between the MRR and the bus waveguide is 1μm. Figure 1(b) is the scanning electron microscope (SEM) image of the cross section of the MRR, the ring and the bus waveguide are both 2μm ×3 μm. A mode transformer (MT) structure is added to in-out port of the MRR and the coupling loss is ~2.5 dB per facet at 1550 nm. Figure 1(c) shows the measured transmission loss of the waveguide and the calculated fundamental transverse magnetic (TM) optical field which is expected to be the SC-forming mode is shown in Fig. 1(d).

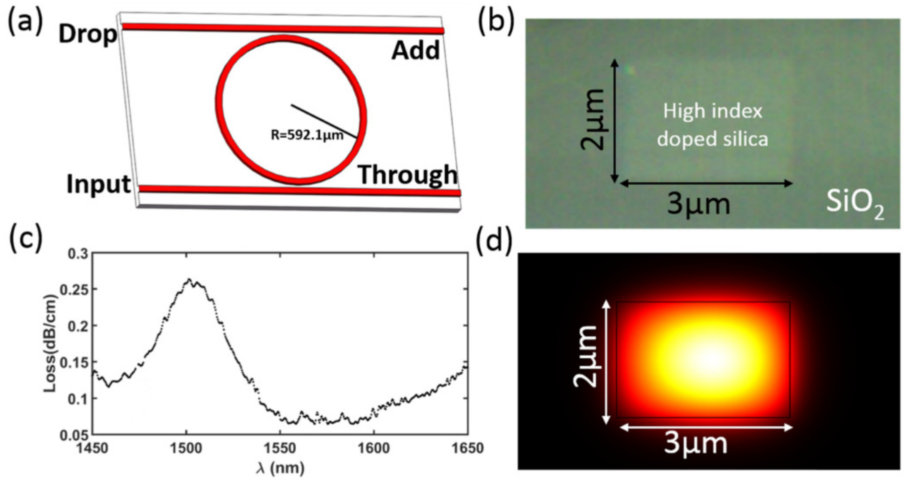

Fig. 1. (a) Schematic illustration of add-drop type MRR. (b) SEM image of the cross section of the MRR. (c) Measured loss parameter versus wavelength. (d) Calculated fundamental TM mode used for generating SC.

Next, the major parameters of the MRR are calculated and analyzed based on the aforementioned parameters. Typically, the deviation of cavity resonance from equidistant spacing can be expressed as [32,33]:

$$D_{\text{int}} = \omega_\mu - \omega_0 - D_1\mu = \frac{1}{2!}D_2\mu^2 + \frac{1}{3!}D_3\mu^3 + \sum_{k>3}\frac{D_k\mu^k}{k!} \tag{1}$$

where ω_μ and ω_0 are resonant and pump angular frequency, μ is the relative mode order. $D_1/(2\pi)$ corresponds to the FSR, $D_2 = -c/n_0D_1^2\beta_2$ illustrates the variation between adjacent FSRs, β_2 is GVD value, c and n_0 are light velocity in vacuum and linear refractive index of this material, respectively. D_3 is third order dispersion (TOD) parameter and D_k (k>3) is higher order dispersion (HOD) coefficients. For our device, $D_2/(2\pi)$ is 175 kHz, the D_{int} curve shown in Fig. 2(a) exhibiting perfect parabolic feature suggests that TOD and HOD can be neglected in this work. Mode interaction between SC-forming mode and interaction-expected mode 2$^{\text{nd}}$ transverse electric (TE) mode (90 × FSR) is also observed from the calculations, which is roughly consistent with previous experimental demonstrations (102 × FSR) [27] and the difference between calculation and experiment is expected to be attributed to thermal effects. Another essential parameter used in subsequent simulation is the nonlinear coefficient: $\gamma = \omega_0n_2/(cA_{\text{eff}})$, where $n_2 = 1.15\times10^{-19}$ m^2/W [28] is the nonlinear refractive index, $A_{\text{eff}} = [\iint|E(x,y)|^2dxdy]^2/[\iint|E(x,y)|^4dxdy]$ is effective mode area with E(x,y) of mode field distribution. The effective mode area, loaded Q, FSR and group index are simulated and presented in Fig. 2(c) and Fig. 2(d), respectively.

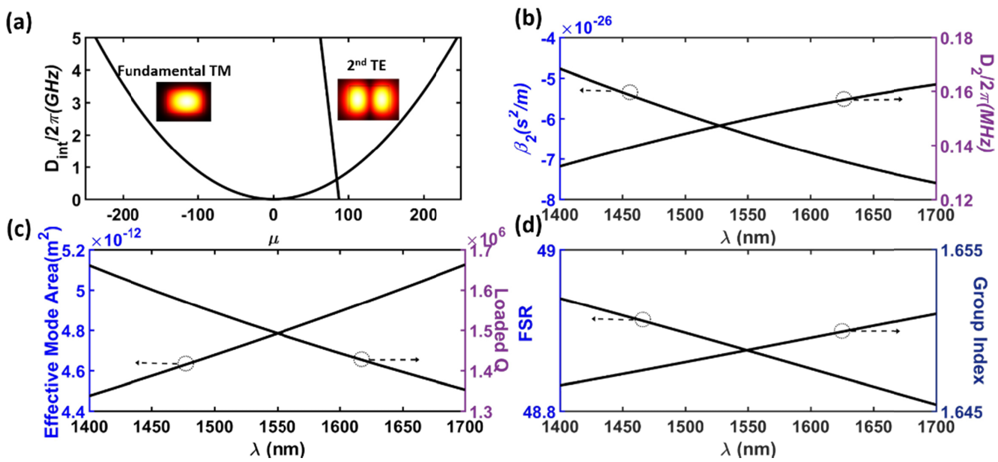

Fig. 2. Calculated major parameters of the MRR. (a) Integrated dispersion curve at pump wavelength (1556.3 nm in experiment), exhibiting perfect parabolic characteristic. The intersection curve belonging to 2nd TE mode induces mode interaction. Insets: calculated optical field of SC-forming and interaction mode. (b) GVD and D_2 curves. (c) Effective mode area and loaded Q value of the MRR. (d) FSR and group refractive group index.

3. Experiments and results

The experimental set-up is shown in Fig. 3. The pump laser is an external cavity diode laser (ECDL) with the linewidth of ~100 kHz at a fixed wavelength of 1556.3nm and boosted by a commercial erbium doped fiber amplifier (EDFA). A fiber polarization controller (FPC) controls the polarization states inside the resonator. The monolithic MRR is pigtailed with a standard fiber array and packaged in a 14-pins butterfly package [27]. The optical spectrum analyzer (OSA) and power meter directly monitors the spectrum and energy inside the MRR. A high precision thermoelectric cooler (TEC) is used to tune the resonance wavelength using the thermo-optic effect.

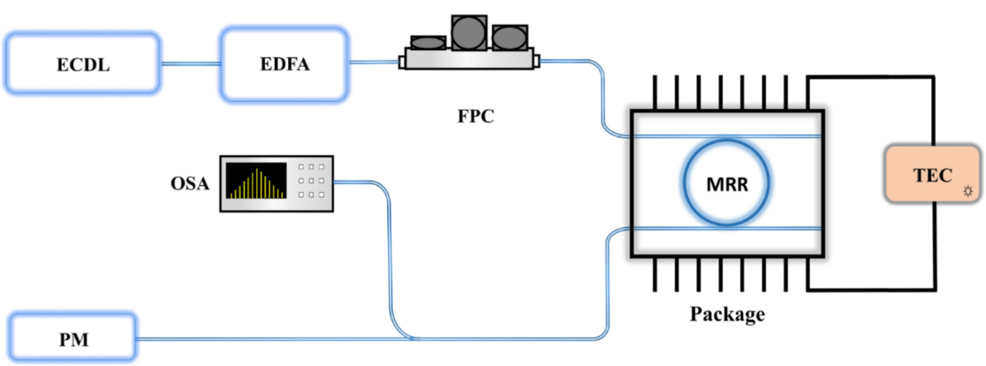

Fig. 3. Experiment set-up of the SC. ECDL: external cavity diode laser. EDFA: erbium doped fiber amplifier. FPC: fiber polarization controller. MRR: micro-ring resonator. TEC: thermos-electric cooler. OSA: optical spectrum analyzer. PM: power meter.

With proper polarization state and pump power (~31.7 dBm in the experiment), primary comb (Turing pattern), chaotic state comb (modulation instability comb) and mode-locked SCs are generated in sequence, as shown in Fig. 4. The case of SC with one vacancy [27] is presented in Fig. 4(c), which presents asymmetric spectrum about the pump from the sech^2 fit line shown in orange. Apparently, the amount of shift could be measured by the difference of center frequency of SC spectrum and the pump frequency. However, for most of SC spectra,

Optical Materials EXPRESS

it is not precise to determine the central wavelength because the defects caused by special distributions of soliton ensembles keeps the spectrum bumpy and uneven. Fortunately, the power difference between symmetric "primary like" comb line with dominant power can be taken as a reference to speculate RSFS effects. Next, the Raman shock time will be analyzed through comparing the theoretical and experimental spectra.

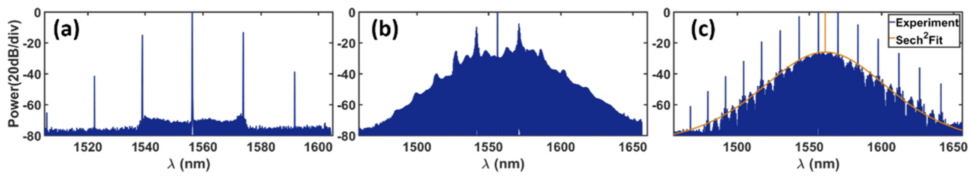

Fig. 4. SC evolution process. (a) Primary comb. (b) MI comb. (c) SC with one soliton out of phase.

4. Model and simulation

The theoretical model to research on the frequency-shift is based on the damped, driven LLE equation augmented by mode-crossing and Raman terms [34,35]:

$$\begin{aligned}&(t_R\frac{\partial}{\partial t}+\frac{\alpha+\kappa}{2}+i\frac{\beta_2 L}{2}\frac{\partial^2}{\partial\tau^2}+i\delta)E-\sqrt{\kappa}E_{in}\\&-i\gamma L(E\int_{-\infty}^{+\infty}R(\tau^{'})\,|\,E(t,\tau-\tau')\,|^2\,d\tau^{'})=0\end{aligned} \tag{2}$$

where $E(t,\tau)$ is the complex slowly varying amplitude of the intra-cavity field with t and τ correspond to slow and fast time evolution of the field, respectively. t_R and α are the round-trip time and intra-cavity losses shown in Fig. 1(c). κ corresponds to power transmission coefficient of the input coupler. δ is the cavity detuning between pump and corresponding resonance. E_{in} is the external pump term and L is the total cavity length. $R(\tau)$ is the nonlinear response of high index doped silica, including Kerr and Raman response [5]. Since the soliton pulse in our experiment is measured to be ~ 120 fs [27] (simulated under the perfect SC case), which is larger than 100 fs [5], thus the Taylor expansion and necessary normalized condition [25] can be applied to simplify the last term in Eq. (2) as:

$$i\gamma L(|\,E\,|^2+\tau_R\frac{\partial\,|\,E\,|^2}{\partial\tau}) \tag{3}$$

where the first term is Kerr effect, and the second term containing Raman shock time τ_R causes the RSFS. Mode-crossing effect is included by adding a phase shift $\Phi_\omega = a/(\omega\text{-}\omega_I)$ to the perturbed modes [36], where a reflects the strength of the interaction and ω_I is the interaction position which locates at around 1517 nm (102 × FSR away from the pump) [27], so the interaction is imposed on the 102nd comb line away from the pump wavelength. Numerical simulation is realized via split-step Fourier algorithm [37] and fourth-order Runge-Kutta method [38]. The wavelength-dependent loss effects are taken into account within the Fourier term during simulation.

In order to stably simulate SCs of our experiment, Gaussian pulse distributed in specific positions determined by experimental spectra is chosen to be the initial condition [39]. During the simulation, there are two critical variables, δ and τ_R. After extensive calculations, δ between 0.015 and 0.0188, τ_R ranging from 2.3 fs to 3.1 fs are effective and consistent with the experimental spectra. Values beyond these ranges are proved to be either unstable or inconsistent with the experiments, for example, Figs. 5(a) and 5(b), Figs. 5(c) and 5(d) show the unstable (δ = 0.018, τ_R = 2.55 fs) and stable crystal (δ = 0.013, τ_R = 2.55 fs) evolution in time and frequency domain with aforementioned parameters, respectively.

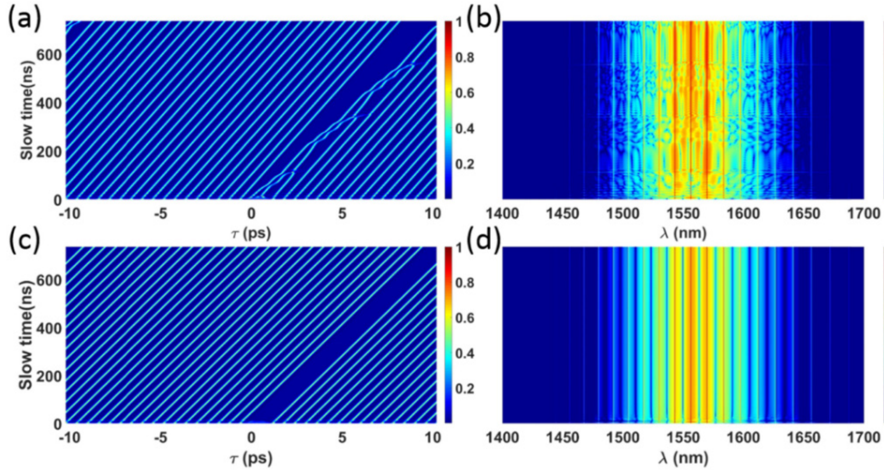

Fig. 5. SC evolution within different condition. Unstable state in (a) time domain and (b) frequency domain with $\delta = 0.013$ and $\tau_R = 2.55$ fs. Stable state in (c-d) shows robust evolution with $\delta = 0.018$ and $\tau_R = 2.55$ fs.

Figure 6 shows the simulation results of 3 different SCs. For each spectrum, different values of τ_R and δ are used to numerically calculate the perturbed LLE, then the power difference between mode + 34 and −34 (first pair of symmetric "prime-comb" modes about the pump) are accumulated. The right column of Fig. 6 presents the power difference variation with different combinations of τ_R and δ, the horizontal dashed lines are their corresponding experimental power difference values. The simulated curve is not effective unless it has intersection points with the dashed line. Note that τ_R and δ beyond the calculation ranges are unstable in the simulation. Figure 6(c) shows that when 2.5 fs < τ_R < 3.1 fs, there are intersections between simulated and experimental spectra. While the range of τ_R is 2.3 fs to 2.5 fs for Fig. 6(f) and 2.3 fs to 2.9 fs for Fig. 6(i). According to these results, 2.5 fs < τ_R <2.7 fs is effective for all the three cases. In further simulation, τ_R = 2.55 fs is selected for Figs. 6(b), 6(e) and 6(h), with varying δ values between the range mentioned above, all the simulated spectra are in good agreement with experiments.

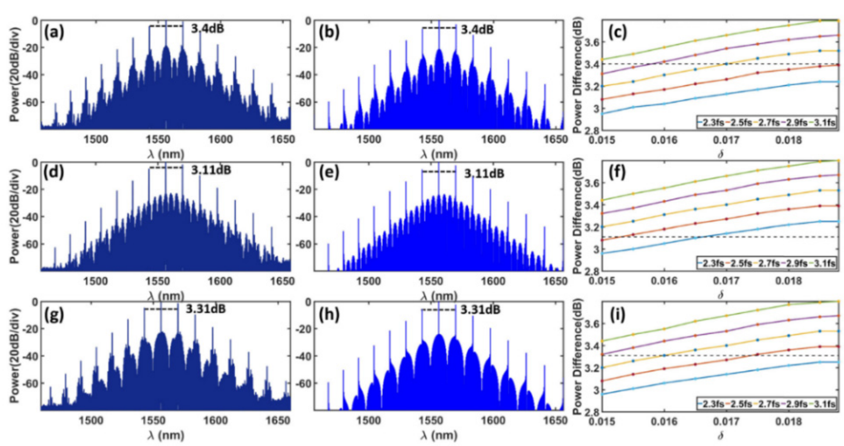

Fig. 6. Experimental (first column) and Simulated spectra (the middle column) with Raman interaction, τ_R = 2.55 fs. (a)-(c) Experimental and simulated SC spectra with "one-gap-peak" feature, experimental power difference is 3.4 dB, δ = 0.0182. (d-f) Spectra present "two-peaks", power difference is 3.11 dB, δ = 0.015. (g-i) Spectra with "Stack" feature with power difference of 3.31 dB and δ of 0.0170. Horizontal dashed lines in (c), (f) and (i) are the corresponding power difference from experiments.

Optical Materials EXPRESS

5. Conclusion

In conclusion, the RSFS of SCs in a high-Q MRR made of high index doped silica is demonstrated. It is precisely researched that the strongly wavelength-dependent loss and RSFS jointly contribute to the asymmetric spectra about the pump. Raman shock time at the range of 2.5 fs to 2.7 fs is inferred by comparing the experiments and the simulations. This work not only improves the modeling accuracy for this material, but also gives reasonable prediction for RSFS on single-soliton that will be researched in the near future.

Funding

National Natural Science Foundation of China (Grant No. 61635013; 61675231; 61475188; and 61705257) and the Strategic Priority Research Program of the Chinese Academy of Sciences (Grant No. XDB24030600).

Acknowledgments

The authors thank T. T. Yu, L. Wang and P. X. Chen for help in the device design.